ISSN 2616-5767 Vol.8, Issue 5: 49-58, DOI: 10.25236/AJETS.2025.080507

Exploring the Control of Paddle Cavitation and Vortex

Chen Zhuo

Oundle School, The Great Hall, New Street, Oundle, PE8 4GH, UK

Abstract: *This investigation focused on the significant issue of energy loss in competitive rowing, where estimates of power losses at the blades were in the order of 20–30% of the rower's power output, due to hydrodynamic inefficiencies, primarily caused by cavitation and turbulence. This project aims to identify key design factors that will improve energy transfer from the oar to the water, thereby enhancing propulsion efficiency and reducing fatigue in the athlete. An experimental station was engineered to provide precise, linear motion of various blade designs through water, with a pressure sensor quantifying force output. This was complemented by high-speed videography using food dye to visualize vortex formation. Advanced computational fluid dynamics simulation software - Flow 3D - is used to analyze the cavitation and turbulence. The simulation could provide details of pressure distribution and flow patterns which are difficult to observe in empirical experiments. The conclusion is delivered through a comparative analysis of both quantitative force data and qualitative flow visualizations. The findings demonstrate that a simulated blade geometry fundamentally overperforms simple shapes by maintaining superior flow attachment, is better at holding water to withstand a stable pressure distribution throughout the stroke. The project successfully connected the theoretical part of hydrodynamics with practical engineering applications, which provided valuable insights for the development of the majority of the rowing community.*

Keywords: *Turbulence, Bubble formation, Energy Loss, Hydrodynamic Inefficiencies, Edge and Surface Modifying*

1. Introduction

1.1 Problem to Solve

In rowing, the force that the athlete outputs are transferred onto the blade and then to the water, pushing the boat forward. During these phases, the energy that the athlete initially exerts cannot be fully transferred into thrust on the blade. The total energy loss from the rower to the oar, then to the water, is approximately 20% to 30%, including 5 to 10% of the energy that is lost when force is exerted on the oar, which will cause slight deformation to the blade, causing some of the energy to dissipate as heat [1]. The primary energy loss in an oar's stroke is not from high-pressure evaporation but from fluid drag and turbulence. As the oar moves, it must push water aside, and "this turbulence results in a powerful, opposing force" known as drag, which acts against the thrust.[2] Furthermore, the described bubble formation is a separate phenomenon called cavitation, which occurs "when the pressure of the liquid is reduced to its vapor pressure," not increased, forming bubbles that collapse inefficiently and reduce propulsion.[3] This could lead to multiple factors that influence the rower. The immediate impact is during high-intensity races, specifically in 2000m (the most common length in rowing races), where continuous energy loss can cause rowers to overexert themselves. If there is a constant 20% energy loss, rowers need to produce 20% extra force to compensate for the loss. This leads to faster fatigue in the rower due to the accelerated blood lactate accumulation, causing a lack of force in the final sprint of the race, which determines the medal. Although the total energy output could be varied through the profession and the strength of the rower, experimenting with the shape of the oar, the roughness on the surface of the oar, and how effective they are will benefit the rowing community, nevertheless.

1.2 Background Information

1.2.1 Shape of the oar

As shown on the right of Figure 1, the general shape of the high-angle blade is large and wide, short

ISSN 2616-5767 Vol.8, Issue 5: 49-58, DOI: 10.25236/AJETS.2025.080507

and rectangular, allowing a big surface area to contact the water. It is widely used for short sprinting races or water with a strong current. The large surface area allows it to hold more water, making it suitable to withstand the strong drive of currents; it increases the water resistance the boat stable while rowing. However, this has the downside of being heavy, which can accelerate physical exhaustion for the rower. Also, its weight makes it hard to control during the race, which might result in an inaccuracy of angle when the oar enters the water surface, creating a big splash of water, causing imbalance and energy waste. This type of blade is mainly used in traditional dragon boat racing.

Figure 1 High-angle and low-angle blade [4]

Figure 2 Spoon blade [4]

On the left of Figure 1, is a type of low-angle blade that essentially follows the opposite design of the high-angle blade; its blade is small but long, and it is more hydrodynamic than the high-angle blade. Due to its lightweight and small surface area, it is suitable for long-distance rowing since it requires less force to row. During the recovery phase, air resistance has a reduced impact, thereby reducing the physical burden. Although it cannot hold as much water while rowing, it is more user-friendly since it does not require accuracy, and rowers do not need to generate much power while rowing. Still in huge waves or currents, it requires high skills to balance the boat since the oar itself is not strong enough to resist violent contact. This type of blade is used most in marathon kayaking races in calm water.

Figure 2 conveys the side and above view of a spoon blade, which is the most common blade type, due to its curved shape, which makes it light but able to hold a decent amount of water while rowing. Its unique shape allows it to reduce its horizontal offset, causing energy loss. Although its spoon-like shape means that the rower can change directions easily, it requires skills and experience in order to utilize its function to its fullest. This type of blade improved the shape from the two above; therefore, in future design, considering this shape of the blade is important to make comparisons on how small changes will affect its performance.

1.2.2 Surface smoothness of the blade and its effect

Different surface processes will alter the friction between the blade surface and the water in contact, causing various phenomena that create different turbulence and bubble formations. A bubble will form due to a large difference in pressure and high friction.

A smooth surface needs a higher velocity to create a bubble, since its low friction reduces the vertical difference in its microstructure, resulting in the force on its surface being distributed evenly, causing a smaller difference in pressure. This shows that bubbles are harder to create on smooth surfaces of the blade, making the blade itself more durable.

However, on a rough surface, sometimes the bumps could be overserved virtually, creating a huge pressure difference from point to point, implying that the force distribution is uneven, making water evaporate faster. The bubbles formed will be concentrated and small, since each of these bumps and cracks on the surface will cause a bubble to form due to its high pressure at that specific point, which is called the Cassie-Baxter effect. On the contrary, the bubble formed on a smooth surface will trigger fewer bubbles to form, but each of them is bigger than on the rough surface. There is gas dissolved in water, which explains that in the bubbles, there is not purely water but contains other components. These uneven surfaces will cause a huge disturbance to not only the water but also the gases in the water[5].

The surface roughness will also affect the turbulence. Turbulence forms due to the change in speed of a fluid while it is flowing. The fast current pulls the slower current towards itself, and the slow current drags the fast current, causing the water in that region to spin and creating turbulence. During rowing, the blade will secure water within this area, but the water current around it remains at the same velocity; the velocity of the water held by the blade is almost static. This change in water speed will cause turbulence to form at the back of the blade.

A blade with high friction will increase the hydrodynamic resistance between the water and the blade.

ISSN 2616-5767 Vol.8, Issue 5: 49-58, DOI: 10.25236/AJETS.2025.080507

While the highly rough surface disturbs the flow of the water, it breaks down turbulence into smaller and more chaotic disorder of water. This will increase the resistance on the blade, resulting in a greater energy loss. The velocity gradient in chaotic vortices will increase, causing the fluid's internal friction to turn from kinetic energy into thermal energy.

On a smooth surface, when fluid flows past, a laminar boundary layer will form; it will suddenly separate due to the adverse pressure gradient, and the shear layer will create a periodic Karman vortex street behind the blade – two alternating vortices that rotate in opposite directions behind the object. This can cause vibrations to the structure due to the big vortices formed, which accelerate the damage to the blade. This will affect the efficiency of the blade itself and cause energy loss.

Lastly, on a low-friction blade, it will hopefully cause a delayed flow separation. Through this, the low-pressure wake zone was reduced, resulting in a significant decrease in the drag of the blade. Sharkskin riblets and golf balls all share the same logic, using controlled surface roughness to optimize the energy transfer and improve efficiency.

1.3 Problem Solving

To discover the factors that will affect the efficiency of the work done on the blade, including the effect on the blade when it is moving underwater, which causes bubbles and vortices to form. This experiment investigates the geometry of the blade through different variables: shapes, surface friction, and contour of the oar. The blade types are in the following: rectangular blade, rectangular blade with unilateral zigzagged edge, rectangular blade with bilateral zigzagged edge, unilateral curved-edged blade, and bilateral curved-edged blade. Also, covering the blade surface with various roughness membranes to determine which surface friction has the most efficient work done with the same force and displacement.

A laboratory station is built to run the experiment; the structural framework is made of 3030 aluminum and utilizes a guide rail control test bench to enable linear movement with precise control of the blade's velocity using a stepper motor. Guide rails employ 20mm steel shafts to ensure the station's strength and rigidity. The testing blade uses an acrylic sheet with applying laser cut to produce simple and flat shapes or uses a 3D printer to produce more complex shapes. Meanwhile, Flow3D, a simulation software, is adopted to run the hydrodynamics analysis by using a full-scale blade model.

1.4 Project Explanation

This project will need to produce a 15 cm-long 3D printed blade, a 5 mm-thick rectangular blade, to ensure the shape and scale of the blade suit the requirements of the experiment. The oar is secured on the rail bracket above a transparent water tank. A stepper motor-driven synchronous belt system is used to achieve a realistic and precise control of the blade movement. With the intention to observe clearly the forming processes of the vortex under water, during the experiment, this project will inject black food colorants and use a 240fps slow-motion to capture the changing vortices at the tip of the blade. To examine and record the distribution of the cavitation bubbles generated through the movement of the blade, this experiment applies an image processing technique to calculate the coverage of the bubbles. It could accurately evaluate the level of damage of the bubble phenomena. Two SolidWorks hydrodynamics simulators, 3D modeling software and Flow 3D, are used in the experiment. The blade model is set up with the same experiment conditions to guarantee the geometric parameters of the model are identical to reality. To mimic the cavitation bubbles in a water current and the features of the turbulence, this experiment set up high mesh density around the edge of the blade and neglected rather insignificant parts with a lower mesh density of mesh. Being selective in setting up the density of the mesh can speed up the simulation but still ensure the quality and accuracy of the outcome. VOF (Volume of Fluid) multiphase model and LES (Large Eddy Simulation) turbulence model are set up, including water and air parameters. The blade is defined to move linearly at a constant speed. The simulation lasts for 2 seconds to obtain detailed flow field information.

1.5 Project Innovation and Significance

Vortices are observed from the diffusion of black food colorants to visualize the strength of the turbulence. This method is easy to operate, also reduces the cost of the project. Food colorant will barely affect the original flow of the water, which protects the reliability of the experiment. This brings easy visualization and provides a new way of quantitative analysis.

A slow-motion camera captures the instantaneous bubble evaporation which completely reveals the

ISSN 2616-5767 Vol.8, Issue 5: 49-58, DOI: 10.25236/AJETS.2025.080507

entire process of how the bubbles developed, formed, and disappeared during rowing. This provides crucial information for the future when achieving the to try to reduce the bubbles produced at the tip of the blade.

Practicality of the project: after verification and improvement of the blade surface, the processing method could be instantly used in competitive rowing events to benefit the rowing community. This project has a practical engineering application value and is expected to enhance the entire rowing efficiency and experience, making the events more competitive and exciting to watch.

2. Theoretical basis

2.1 Momentum equations

The equations of motion for the fluid velocity components (U, V, W) in the three coordinate directions are the Navier-Stokes equations with some additional terms:

$$\begin{aligned}
&\frac{\partial u}{\partial t}+\frac{1}{V_F}\left\{uA_x\frac{\partial u}{\partial x}+vA_yR\frac{\partial u}{\partial y}+wA_z\frac{\partial u}{\partial z}\right\}-\xi\frac{A_yv^2}{xV_F}=-\frac{1}{\rho}\frac{\partial p}{\partial x}+G_x+f_x-b_x-\frac{R_{\mathrm{SOR}}}{\rho V_F}(u-u_w-\delta u_s)\\
&\frac{\partial v}{\partial t}+\frac{1}{V_F}\left\{uA_x\frac{\partial v}{\partial x}+vA_yR\frac{\partial v}{\partial y}+wA_z\frac{\partial v}{\partial z}\right\}+\xi\frac{A_yuv}{xV_F}=-\frac{1}{\rho}\left(R\frac{\partial p}{\partial y}\right)+G_y+f_y-b_y-\frac{R_{\mathrm{SOR}}}{\rho V_F}(v-v_w-\delta v_s)\\
&\frac{\partial w}{\partial t}+\frac{1}{V_F}\left\{uA_x\frac{\partial w}{\partial x}+vA_yR\frac{\partial w}{\partial y}+wA_z\frac{\partial w}{\partial z}\right\}=-\frac{1}{\rho}\frac{\partial p}{\partial z}+G_z+f_z-b_z-\frac{R_{\mathrm{SOR}}}{\rho V_F}(w-w_w-\delta w_s)
\end{aligned}\tag{1}$$

In the equations above, the variables are receptively: (G_x, G_y, G_z) are body accelerations; (f_x, f_y, f_z) are viscous accelerations; $\mathbf{U}_w=(u_w,v_w,w_w)$ is the velocity of the source component; $\mathbf{U}_s=(u_s,v_s,w_s)$is the velocity of the fluid at the surface of the source relative to the source itself. It is computed in each control volume as:

$$\mathbf{U}_s=\frac{dQ}{\rho_Q dA}\mathbf{n}\tag{2}$$

dQ is the mass flow rate; ρ_Q is the fluid source density; dA is the area of the source surface in the cell, and 'n' is the outward normal to the surface.

At a stagnation pressure source, fluid is assumed to enter the domain at zero velocity. As a result, pressure will build up at the source and move the fluid away from the source. At a static pressure source, the fluid velocity is computed from the mass flow rate and the surface area of the source. In this case, no extra pressure is required to propel the fluid away from the source. Note that the static or stagnation pressure property does not apply to negative mass sources, i.e., sinks.

For a variable dynamic viscosity (μ), the viscous accelerations are

$$\begin{aligned}
\rho V_F f_x &= wsx-\left\{\frac{\partial}{\partial x}(A_x\tau_{xx})+R\frac{\partial}{\partial y}(A_y\tau_{xy})+\frac{\partial}{\partial z}(A_z\tau_{xz})+\frac{\xi}{x}(A_x\tau_{xx}-A_y\tau_{yy})\right\}\\
\rho V_F f_y &= wsy-\left\{\frac{\partial}{\partial x}(A_x\tau_{xy})+R\frac{\partial}{\partial y}(A_y\tau_{yy})+\frac{\partial}{\partial z}(A_z\tau_{yz})+\frac{\xi}{x}(A_x+A_y\tau_{xy})\right\}\\
\rho V_F f_z &= wsz-\left\{\frac{\partial}{\partial x}(A_x\tau_{xz})+R\frac{\partial}{\partial y}(A_y\tau_{yz})+\frac{\partial}{\partial z}(A_z\tau_{zz})+\frac{\xi}{x}(A_x\tau_{xz})\right\}
\end{aligned}\tag{3}$$

2.2 Viscosity Evaluation

In single-fluid or two-fluid models, dynamic viscosity (μ) can be assigned constant values for each fluid component. For mesh cells containing a mixture, viscosity is computed as a volume fraction-weighted average of these constants. This approach is beneficial in multiphase flows where different fluids interact, such as in oil-water systems or gas-liquid flows. In the single-fluid model, even if the fluid consists of two components (each with distinct densities and viscosities), the mixture viscosity is still evaluated as a weighted average. Furthermore, when dealing with partially solidified fluids, viscosity may also depend on the solid fraction, incorporating phase-change effects. When turbulence is considered, the effective viscosity is the sum of the molecular viscosity (μ) and turbulent viscosity (μ_t). For non-Newtonian fluids, viscosity is not constant but varies with strain rate and temperature. FLOW-3D employs a generalized form of the Carreau model to describe strain-rate-dependent viscosity:

Where:

γ is the strain rate magnitude; μ0 and μ∞ are zero and infinite shear-rate viscosities; λ is a time

ISSN 2616-5767 Vol.8, Issue 5: 49-58, DOI: 10.25236/AJETS.2025.080507

constant; n is the power-law index; f(T) represents temperature dependence.

$$\mu = \mu_\infty + (\mu_0 - \mu_\infty)\left[1 + (\lambda\dot{\gamma})^2\right]^{\frac{n-1}{2}} \cdot f(T)$$

The temperature correction factor is given below. and a, T, and T_0 are constants.

$$f(T) = \exp\left[a\left(\frac{1}{T - T^*} - \frac{1}{T_0 - T^*}\right)\right]$$

2.3 Baffle Flow Losses

Porous baffles introduce flow resistance, which is modeled in FLOW-3D using a pressure loss equation. For flow in the x-direction, the loss term is:

$$\Delta p_x = \left(\frac{\mathrm{KBAF1}}{P_{\mathrm{BAF}}} + \mathrm{KBAF2} \cdot \frac{u_{\mathrm{micro}}}{2}\right)\frac{\Delta x}{P_{\mathrm{BAF}}} \cdot u_{\mathrm{micro}}$$

KBAF1 (velocity units) and KBAF2 (dimensionless) are input coefficients; P_{BAF} is the baffle porosity; Δx is the distance between pressure nodes; u_{micro} is the microscopic velocity inside the porous medium; The microscopic velocity (u_{micro}) is the actual fluid velocity within the pores, whereas the bulk velocity is the apparent velocity used in macroscopic flow equations.

The baffle model ensures that the pressure drop (Δp) remains consistent regardless of mesh resolution. For a constant flow speed, the pressure drop is shown below. This formulation guarantees that simulations produce physically realistic results without mesh dependency.

$$\Delta p = \left(\frac{\mathrm{KBAF1}}{P_{\mathrm{BAF}}} + \mathrm{KBAF2} \cdot \frac{u_{\mathrm{micro}}}{2}\right) \cdot u_{\mathrm{micro}}$$

2.4 Fluid Energy Equations

For compressible or thermally active flows, FLOW-3D solves the internal energy equation to account for heat transfer and thermodynamic work. The macroscopic mixture internal energy E is governed by:

$$\frac{\partial(\rho E)}{\partial t} + \nabla \cdot (\rho \mathbf{u} E) = -p\nabla \cdot \mathbf{u} + \nabla \cdot (k\nabla T) + \Phi$$

$$E = \alpha_1 E_1 + \alpha_2 E_2$$

Where: ρ is the fluid density; u is the velocity vector; p is pressure; k is thermal conductivity; T is temperature; Φ represents viscous dissipation. In two-fluid systems, the energy equation incorporates volume fractions (α_1, α_2) to distinguish between phases. Here, E_1 and E_2 are the internal energies of Fluid #1 and Fluid #2, respectively.

2.5 Bubble and Void Region Models

These regions maintain a fixed pressure, such as atmospheric conditions, making them suitable for open-air simulations. The pressure p remains constant over time: $p = p_{atm}$. This simplification is useful when gas dynamics have negligible effects on the overall flow behavior. Cavitation occurs when the local pressure drops below a critical cavitation pressure, p_{cav}, leading to vapor bubble formation. FLOW-3D offers two models for cavitation growth:

2.5.1 Simplified Model

The void fraction increases linearly over time, controlled by the parameter CAVRT. f_{cav} is the cavitation volume fraction.

$$\frac{df_{\mathrm{cav}}}{dt} = \mathrm{CAVRT} \cdot (p_{\mathrm{cav}} - p)$$

2.5.2 Empirical Model

This model incorporates turbulent kinetic energy (k) and surface tension (σ) for a more detailed representation:

Production Rate (bubble formation due to pressure drop):

ISSN 2616-5767 Vol.8, Issue 5: 49-58, DOI: 10.25236/AJETS.2025.080507

$$\text{Production Rate} = C_{\text{prod}} \sqrt{\frac{k}{\sigma}} (p_{\text{cav}} - p) \cdot (1 - f_{\text{cav}})$$

Dissipation Rate (bubble collapse due to pressure recovery); C_{prod} and C_{diss} are empirical constants.

$$\text{Dissipation Rate} = C_{\text{diss}} \cdot f_{\text{cav}}$$

2.5.3 Boundary Effects

Pressure Boundaries: Void regions adjacent to pressure boundaries adopt the prescribed boundary pressure. Velocity Boundaries: Affect enthalpy flux, influencing inflow and outflow conditions. The section above uses the equations and is all referenced to the equation section from the software flow 3D's help page: file:///F:/flow3d/help/theory.html

3. Physical Experiment

3.1 Experimental Station

During simple experiments, although there are different shapes of blades but when pushing them in water, it is hard to get each of them to be at the same velocity, and the water resistance could only be obtained through feeling. These additional variables will make the experiment less reliable and accurate; therefore, an experimental station with a stepping motor is built to control the velocity of the moving blade and two guiding rails to secure the vertical position during rowing, guaranteeing that the blade is moving in a linear motion and providing extra support to the station. This station enhanced the stability and the rigidity of the experiment and made steady speed variation an easier approach. Adding the pressure sensor on the blade makes the data reflection more accurate, and it not only relies on feeling, but also allows a graph can be easily drawn with this data. This will make the results more presentable and easier to visualize and compare during the data analysis.

In the sport of rowing, once the blade enters the water, it acts as an anchor to the boat, holding and withstanding the water resistance, pushing the boat forward without changing its general position in the water; from the catch to feathering the blade angle will change locally. However, in our experiment, the water is static with the blade moving in water, and the turbulence is created through the horizontal movement of the blade, whereas in rowing, the turbulence is mainly produced through the change in angle of the blade in water, not due to speed.

3.2 Electronics

To detect the pressure on the blade during rowing, the experiment uses the HX711 pressure sensor to collect the force exerted on the blade and analyze the effect on each different shape. To monitor pressure data in real time, an HX711 load cell amplifier with an Arduino microcontroller is connected to the system to a computer. The Arduino was programmed to read and transmit sensor data through the Serial Monitor, enabling real-time observation and recording of pressure variations.

To ensure the constant velocity of the blade moving in the water, A PLE 42 -50 stepper motor is used and is connected to the Arduino Uno control board, which has the code with instructions for the motor. This way, the speed of the blade moving in the water is controllable through the software 'blinker' on a phone. Using Arduino to code and name all the buttons that will be used during the experiment, this avoids changing the code every time if one wishes to test another movement speed, which reduces the chance of mistakes and improves the efficiency of the experiment.

The controlling board of the stepper motor on the application is 'Blinker'. The buttons include clockwise and anticlockwise options with speeds of 4000, 4200, and 4300; the button 'stop' is used to prevent damage to the motor from sudden changes in direction while working. All of actions will be presented in the monitor above in order to allow you to review the data.

The serial port monitor is to convert data into numerical values and draws a graph for straightforward comparison between data sets. The data could be displayed in many forms: binary, hexadecimal, ASCII, and UTF-8. Each time the cable is connected to the computer, the data will start generating 10 times each second. This assures the data to be constant and reflective, making the graph a continuous line with clear variations. The increase in numbers will reduce the effect of incorrect values on the entire data set of the experiment.

ISSN 2616-5767 Vol.8, Issue 5: 49-58, DOI: 10.25236/AJETS.2025.080507

3.3 Method

1. Fill the water tank with enough water to at least cover half of the blade underwater. 2. Change the blade type on the pressure sensor to examine a different blade from the last one, and secure it with four bolts, making sure that it will not fall off during the experiment. 3. Connect the Arduino Mega control board to the serial port of the computer to read the data from the pressure sensor connected to the blade on the serial port monitor. Set the time interval for returning data to 1ms, ensuring that the data reflection is instantaneous. 4. Connect the Bluetooth module of the motor to the app 'Blinker', which allows me to control the speed and the directions of the motor, and when to stop due to the code. Connect the battery to the motor to provide energy. 5. Set up the camera in slow motion to capture the details of the water movement. 6. Add a few drops of black food coloring to the water next to the blade to observe the vortices created by the blade and compare the differences. 7. Collect the data from the pressure sensor that connects with the blade and draw a graph using the graphing function in the serial port monitor. 8. Undo the blots and take off the blade. Change to another blade and repeat steps 2-7.

4. Simulation

Create a new file and add a new simulation. Set up all the physics parameters so that the simulation can run properly without reporting an error. (The parameters that are chosen due to the requirements of emphasizing turbulence and bubbles during rowing: bubble and phase change, cavitation, density evaluation, gravity and non-inertial reference frame, heat transfer, and viscosity and turbulence.)

Then set the fluid as water at 20 degrees Celsius. Choose one of the STL files that is previously modeled in SolidWorks and transfer the unit from millimeters to meters (SolidWorks uses mm as the unit of length, and Flow3D uses m as the unit of length). The numerical size in the STL file follows the unit in SolidWorks; therefore, we need to maintain the proportionality of the model.

After the model is successfully transferred to flow3D, set up the mesh to tell the software how detailed we want the analysis to be. The more detailed the mesh is, the longer it will take the simulation to run. Therefore, applying a sparse mesh to cover the region around the model allows a decent amount of water to run. However, on the edge of the blade, create a denser mesh to allow a detailed breakdown of the blade when in contact with water. This action not only reduced the time of the simulation but also assured the accuracy of the simulation.

After the simulation runs out, generate an animation for a clearer view of different blades in water. The color of the water refers to the water pressure in the region, and when it changes color, it indicates the effect of the blade on the water.

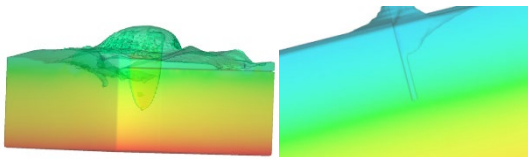

(1) *(2)*

Figure 3 Bubble formation

As shown in Figure 3 (1) and (2) above, the observation is that a bubble formed at the tip of the blade and the turbulence behind the blade when water is disturbed. This simulator will use detailed calculations to generate multiple images, and by connecting all the images, the animations will be formed. This gives a chance to observe each image in detail before the animation is created. Allow zooming in and out to investigate the changes in the water in a microscopic way. However, an area not around the blade with a sparse mesh might cause inaccuracy of the water flow, and when zoomed in, the water flow might not be smooth like a fluid, which might cause the general effect of the animations not to be ideal due to lagging.

5. Data Analyzation

5.1 Data from physical experiment

The primary objective of constructing this experimental station was to avoid the inaccuracy of manual feelings and move to reliable and quantitative data on hydrodynamic performance. Through using the

ISSN 2616-5767 Vol.8, Issue 5: 49-58, DOI: 10.25236/AJETS.2025.080507

stepper motor to enforce a constant velocity and the guiding rails to ensure strictly linear motion, the variables of human inconsistency were eliminated. This setup allowed the HX711 pressure sensor to function as a precise measuring instrument, translating the complex interaction between blade and water into a clear, numerical dataset. The real-time graphing function of the serial port monitor was instrumental, as it provided an immediate visual representation of each blade's force profile, making comparative analysis both efficient and objective.

The analysis of the serial output graphs will reveal a fundamental difference in how each blade design interacts with water during rowing. From Figures 4 and 5, the standard rectangular and the zigzag-edged blades (both sided and single-sided), the data directly shows both blades' inefficiency. The graph line shows an immediate and violent spike in force when the motor is initially moved, rapidly reaching the upper limit, between around 42-57g (Absolute value, where negatives are the direction, not the magnitude of the force). However, this peak is not sustainable; within milliseconds, the data line undergoes a catastrophic drop, often plummeting to values at or below 20g and remaining there for the rest of the stroke. This is the case with all three speed variations, and the greater the speed on average, the bigger the values will get, but the difference for the drastic drop remains generally the same. The high initial peak represents the blade slapping against the water's surface, while the subsequent drop quantifies the energy lost to the formation of a large, low-pressure cavity filled with bubbles and turbulent vortices directly behind the blade. The blade, in effect, is pulling its chaotic wake through the water, which requires significant force but generates limited useful propulsion to push the boat further.

Figure 4 The rectangular blade Figure 5 The zigzag-edged blade

Figures 6 represents the cured blade, the performance of the curved arc blades represented a measurable improvement, which was evident in both the data and the visual recordings. Their force profile was characterized by a slightly less sudden ramp-up, reaching a lower peak force of approximately 38-42g. This less aggressive entry reduced the impact shock of the blade. Furthermore, the decline in force was less significant, with the line typically stabilizing around a 25-28g range. This sustained higher force value indicates that the curved geometry promotes better flow attachment around the blade surface, reducing the scale of flow separation and energy-wasting vortices compared to rectangular blades. However, the persistent downward slope of the data line confirms that flow separation, while mitigated, is not prevented. These blades still experience a measurable loss of grip, indicating that their design is a compromise rather than an optimal solution, but they are certainly more effective compared to the rectangular blades.

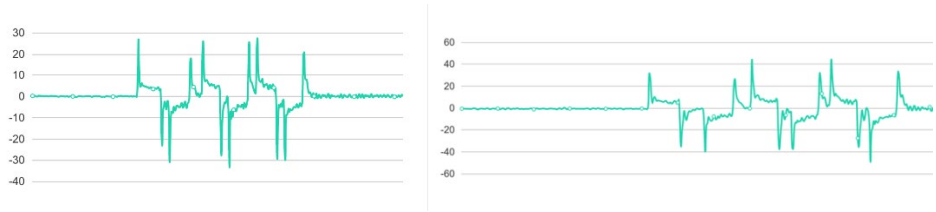

(1) *(2)*

Figure 6 The results of curved arc blades

According to Figure 6 (2), the data output for the simulated 3D printed sculling blade was fundamentally different and superior. Its graph still includes a sharp, transient peak reaching around 90-110g; this is an inevitable start, since when the water and the blade are at rest, a force applied causes the instantaneous acceleration to be large enough to reach the motor's set. Crucially, unlike the other blades, it does not lose this grip; it maintains a very strong and stable force of around 50g for the majority of the stroke. This high, sustained force plateau—significantly higher than the 25-28g of the curved blades—demonstrates its superior ability to hold onto a solid volume of water without cavitation. Therefore, its elite performance comes from generating more power throughout the entire stroke, not from a smoother profile, proving that its evolved geometry is fundamentally more effective at managing flow and converting effort into propulsion.

The qualitative observations from the high-speed camera and food dye provide the perfect visual

ISSN 2616-5767 Vol.8, Issue 5: 49-58, DOI: 10.25236/AJETS.2025.080507

explanation for this quantitative data. For the inefficient blades, the dye was instantly churned into a cloudy, frothy mess, visually mapping the large, chaotic vortices that the sensor measured as a collapsing force line. As shown in Figure 7, for the simulated blade, the dye streamed around its contours in an organized manner, coalescing into two tight, coherent tip vortices with a notably clear and stable flow field directly behind the blade. This clean flow visualization directly correlates to the stable, high-force plateau recorded by the sensor.

Figure 7 The simulated blade

5.2 Simulation Data Analysis

The Flow3D simulation provided a powerful digital counterpart to the physical experiments, enabling me to have a more detailed examination of fluid interactions that are difficult to observe directly with eyes. By configuring key physics modules, including cavitation, turbulence, and multiphase flow, the simulation could accurately model the complex hydrodynamic behavior of each blade type and analyze the contact microscopically.

(1) *(2)*

Figure 8 The pressure distribution and flow patterns

In Figure 8, the analysis of pressure distribution and flow patterns revealed critical differences in performance. For the standard rectangular and zigzagged blades, the simulation showed an immediate formation of a large, unstable low-pressure zone on the rear face. This cavitation zone, visible as a swirling cloud of vapor bubbles in the phase change module, directly corresponds to the dramatic force drop. The pressure plotter showed obvious fluctuations, with rapid transitions from high-pressure (red zones) to low-pressure (deep blue zone) areas, indicating severe flow separation and energy loss through vortices forming and bubbles.

From Figure 9, the curved-edge blade design improved slightly in performance in the simulation. The low-pressure region was more stable, forming further downstream from the blade surface. This resulted in a smoother pressure transition from high to low and reduced cavitation, matching the experimental data showing a more gradual force decline. However, the energy loss is still visible with some clear, big vortices and bubbles at the tip of the double curved-edged blade. Still, the turbulence models result in smaller vortices compared to the rectangular blades.

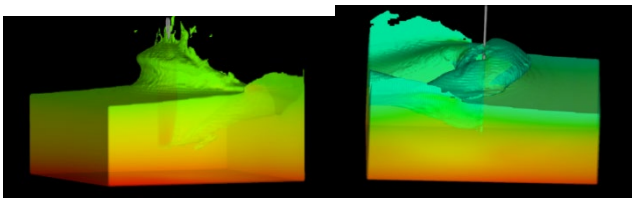

Figure 9 The curved-edge blade design *Figure10 The sculling blade design*

Reflected through Figure 10, the simulated sculling blade showed exceptional performance in the simulation. The pressure distribution remained remarkably stable throughout the motion, with minimal pressure fluctuation and no significant cavitation. The flow remained attached to the blade surface for most of the stroke, with separation only occurring cleanly at the trailing edge. The turbulence models still showed energy loss; however, with the same force exerted, the simulated blade can generate most power back to the water, which is the force that is useful for the movement of the boat. These simulation results provide a perfect explanation for the physical sensor's consistent force readings - the blade maintains optimal pressure distribution throughout its motion.

ISSN 2616-5767 Vol.8, Issue 5: 49-58, DOI: 10.25236/AJETS.2025.080507

The mesh sensitivity analysis confirmed that while the sparse background mesh sometimes produced fewer smooth animations in far-field areas, it had a negligible impact on the critical flow phenomena around the blade itself. The dense mesh surrounding the blade successfully captured all essential boundary layer effects and pressure gradients, ensuring the accuracy of the core findings.

The strong correlation between simulation results and experimental data validates both approaches. The simulation's detailed visualization of pressure distribution and flow patterns provides the perfect explanation for the quantitative force measurements obtained experimentally. Together, they demonstrate that the simulated sculling blade's performance superiority stems from its ability to maintain stable flow attachment and optimal pressure distribution throughout the stroke cycle.

6. Conclusion

6.1 Data collection

This investigation conclusively demonstrates that optimizing blade geometry is significant for modifying the hydrodynamic energy losses—primarily through cavitation and turbulence—that affect competitive rowing. Through rigorous methods of controlled physical experimentation and advanced computational fluid dynamics (CFD) using the simulator – Flow3D, the study validated that an evolved, sculling-inspired blade design fundamentally outperforms conventional shapes. Unlike traditional blades that suffer from catastrophic flow separation and energy transfer inefficiency, the optimized geometry maintains superior flow attachment and stable pressure distribution, thereby translating a greater thrust of the athlete's effort into a sustained, useful push to the water.

6.2 Improvement in the future

In the future, the experiment could simulate the real action of the blade during rowing, where the blade acts as a pivot in the water to push the boat further. Through this, the analysis of the length of the blade and its effect on the movement of the blade could be made, since most of the force pushing the boat forward comes from the moment (rotational force) of the blade. If possible, a blade that is better suited for engineering mechanics to reduce the energy loss and be able to hold more water during rowing could be designed. Future studies could invite rowers to use full-scale blades to physically experience the difference of various types of blades. The practical results are able to provide more persuasive and influential conclusions.

References

[1] Hofmijster, Mathijs, Jos de Koning, and A. J. van Soest. "Estimation of the Energy Loss at the Blades in Rowing: Common Assumptions Revisited." Journal of Sports Sciences, vol. 28, no. 10, Aug. 2010, pp. 1093–1102. http://bionics.seas.ucla.edu/education/Rowing/Rigging_2010_01.pdf#:~:text=In%20rowing%2C%20power%20is%20inevitably%20lost%20as%20kinetic%20energy.

[2] "What Is Drag?" Khan Academy,www.khanacademy.org/science/physics/fluids/fluid-dynamics/a/what-is-drag. Accessed 28 Oct. 2025.

[3] Sponsored Post. "High Angle versus Low Angle Paddling Styles and Why Angle Matters for Sea Kayaking." Paddling Life, 14 Apr. 2020, paddlinglife.com/sea-kayaking/high-angle-versus-low-angle-paddling-styles-and-why-angle-matters-for-sea-kayaking/.

[4] Grapeview Point Boat Works. Oars. https://grapeviewpointboatworks.com/order_oars.html. Accessed 28 Oct. 2025.

[5] Hall, Nancy. "Cavitation." NASA Glenn Research Center, NASA, 5 May 2021, www1.grc.nasa.gov/beginners-guide-to-aeronautics/cavitation/.